Introduction

We focus our attention on modeling frictional contact mechanics coupled with hydraulically active fractures. Fluid flow and poromechanical deformation processes in fractured porous media are strongly coupled: the fluid pressure acts as a normal forcing term on the fracture surfaces, and the conductivity of the fracture is a nonlinear function of the effective aperture. The main challenge is to solve a lubricated frictional contact problem (Wriggers, 2006).

In the literature, many approaches have been proposed to numerically model a discontinuity. They can be grouped in three main classes based on:

- explicit representation, such as Discrete Fracture Model (DFM) and models that use thin layers of continuum finite elements with plastic behavior (Garipov et al., 2016; Rutqvist et al., 2002));
- embedded representation, for example Embedded Discrete Fracture Models (EDFM) and Extended Finite Elements Methods (XFEM) (Shakiba and Sepehrnoori, 2015; Deb and Das, 2010; Deb and Jenny, 2017));
- regularized field representation within a continuum discretization, like Phase Field and damage-mechanics-based approaches (Verhoosel and de Borst, 2013; Wheeler et al., 2014)).

In this work, we use a conforming discretization with interface elements (Goodman et al., 1968) to explicitly represent the fracture. The Karush-Kuhn-Tucker (KKT) conditions need to be enforced for both normal impenetrability and frictional compatibility. The most common techniques to impose these conditions are penalty and Lagrange multiplier methods (Kikuchi and Oden, 1988; Laursen, 2003; Wriggers, 2006). In essence, a penalty-based approach imposes approximate constraints using stiff springs to connect opposite nodes/faces. It does not add any degree of freedom but introduces a source of ill-conditioning. In contrast, a Lagrange multiplier method adds new primary unknowns (the tractions) and changes the global structure of the linear system, but it enforces the constraints in an exact way. We adopt the Lagrange multiplier method.

Based on a single conforming mesh, the displacement field in the rock matrix is approximated by lowest-order continuous finite elements, while the flow discretization relies on a classic cell-centered finite volume approach using a two-point flux approximation (TPFA) scheme for the numerical flux. Because of the coupling between fracture contact and flow processes, it is natural to use piecewise-constant equal-order interpolation of Lagrange multipliers and fluid pressure. Unfortunately, this mixed finite-element/finite-volume scheme is not uniformly inf-sup stable (Wohlmuth, 2011) and requires the implementation of a stabilization methodology. In this work, we first adopt a stabilizing modification of the mass balance and constraint equations based on a macroelement analysis (Silvester and Kechkar, 1990). Then, we propose a novel global jump stabilization that is constructed using a finite volume logic. The proposed stabilization builds on the methods presented in Franceschini et al. (2020), but we formulate a new scheme with some appealing features.

Problem statement and numerical model

Governing equations

An elastic, closed, domain $\overline{\Omega} = \Omega \cup \partial\Omega$ in $\mathbb{R}^3$, with Ω an open set, $\partial\Omega$ its boundary, and $\boldsymbol{n}_\Omega$ its outer normal vector is considered (Fig. 1a). The fracture is described as an internal boundary Γ_f, consisting of two overlapping surfaces Γ_f^- and Γ_f^+, and having orientation $\boldsymbol{n}_f = \boldsymbol{n}_f^- = -\boldsymbol{n}_f^+$ (Fig. 1b). The pressure field is defined on this lower-dimensional domain. For simplicity, we consider the matrix impermeable. To denote the closed domain occupied by the fracture we use $\overline{\Gamma}_f = \Gamma_f \cup \partial\Gamma_f$, with Γ_f a two-dimensional (2D) open surface and $\partial\Gamma_f$ a one-dimensional (1D) curve defining its boundary. The fracture outer normal vector for Γ_f is $\boldsymbol{m}_f$ (Fig. 1c). Finally, $\mathbb{T} = (0, t_{\max})$ is the time domain of interest. Quasi-static

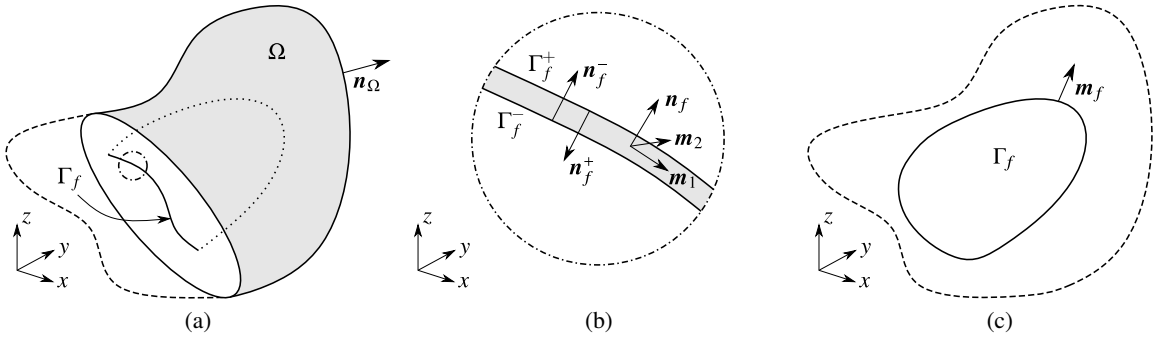

Figure 1: Conceptual scheme for fracture modeling (a); local reference frame on the discontinuity surface (b); and the scheme for the flow domain (c).

conditions and infinitesimal strains are assumed in this work. The fluid is taken to be incompressible, and body force and buoyancy effects are neglected.

The strong form of initial boundary value problem (IBVP) consists of finding the displacement vector $\boldsymbol{u} : \overline{\Omega} \times \mathbb{T} \to \mathbb{R}^3$ and the pore pressure $p : \overline{\Gamma}_f \times \mathbb{T} \to \mathbb{R}$ such that:

$$-\operatorname{div} \boldsymbol{\sigma}(\boldsymbol{u}) = \mathbf{0} \quad \text{in } \Omega \times \mathbb{T} \quad \text{(linear momentum balance)}, \tag{1a}$$

$$\dot{g}_N(\boldsymbol{u}) + \operatorname{div} \boldsymbol{q}(\boldsymbol{u}, p) = q_s \quad \text{in } \Gamma_f \times \mathbb{T} \quad \text{(mass balance)}, \tag{1b}$$

$$\boldsymbol{\sigma}(\boldsymbol{u}) \cdot \boldsymbol{n}_f - p\boldsymbol{n}_f = \mathbf{0} \quad \text{on } \Gamma_f \times \mathbb{T} \quad \text{(traction balance on the fracture)}, \tag{1c}$$

subject to the constraints

$$t_N = \boldsymbol{t} \cdot \boldsymbol{n}_f \leq 0 \quad \text{on } \Gamma_f \times \mathbb{T} \quad \text{(normal contact conditions)}, \tag{1d}$$

$$g_N = [\![\boldsymbol{u}]\!] \cdot \boldsymbol{n}_f \geq 0 \quad \text{on } \Gamma_f \times \mathbb{T}, \tag{1e}$$

$$t_N g_N = 0 \quad \text{on } \Gamma_f \times \mathbb{T}, \tag{1f}$$

$$\|\boldsymbol{t}_T\|_2 - \tau_{\max}(t_N) \leq 0 \quad \text{on } \Gamma_f \times \mathbb{T}, \quad \text{(Coulomb frictional contact conditions)}, \tag{1g}$$

$$\dot{\boldsymbol{g}}_T \cdot \boldsymbol{t}_T - \tau_{\max}(t_N) \|\dot{\boldsymbol{g}}_T\|_2 = 0 \quad \text{on } \Gamma_f \times \mathbb{T}, \tag{1h}$$

with appropriate initial and boundary conditions. To complete the description, we introduce the following symbols, variables, and constitutive relationships:

- $\boldsymbol{\sigma}(\boldsymbol{u}) = \mathbf{C} : \nabla^s \boldsymbol{u}$ is the Cauchy stress tensor, which is related to $\boldsymbol{u}$ by the fourth-order elasticity tensor $\mathbf{C}$, with ∇^s the symmetric gradient operator;
- $\boldsymbol{q}(\boldsymbol{u}, p) = -\dfrac{C_f(\boldsymbol{u})}{\mu} \nabla p$ is the fluid volumetric flux in the fracture domain with ∇p the fluid pressure gradient, μ the fluid viscosity (constant), and C_f the isotropic fracture hydraulic conductivity modeled as in Garipov et al. (2016):

$$C_f = C_{f,0} + \frac{g_N^3}{12}. \tag{2}$$

  $C_{f,0}$ is the initial conductivity associated with two rough surfaces in contact.
- $\boldsymbol{t} = \boldsymbol{\sigma} \cdot \boldsymbol{n}_f^- = -\boldsymbol{\sigma} \cdot \boldsymbol{n}_f^+ = (t_N \boldsymbol{n}_f + \boldsymbol{t}_T)$ is the traction vector over Γ_f, with t_N and $\boldsymbol{t}_T = (t_{m_1} \boldsymbol{m}_1 + t_{m_2} \boldsymbol{m}_2)$ its normal and tangential component, respectively, with respect to the local reference system shown in Fig. 1b;
- $\tau_{\max} = c - t_N \tan(\theta)$ is the limit value for the modulus of $\boldsymbol{t}_T$ according to the Coulomb criterion, with c and θ the cohesion and friction angle, respectively;
- $[\![*]\!]$ denotes the jump of a quantity across Γ_f, with $[\![\boldsymbol{u}]\!] = (\boldsymbol{u}|_{\Gamma_f^+} - \boldsymbol{u}|_{\Gamma_f^-}) = (g_N \boldsymbol{n}_f + \boldsymbol{g}_T)$ the relative displacement across Γ_f, where g_N and $\boldsymbol{g}_T$ are normal and tangential components, respectively, and $\boldsymbol{u}|_{\Gamma_f^+}$ and $\boldsymbol{u}|_{\Gamma_f^-}$ are the restrictions of $\boldsymbol{u}$ on Γ_f^+ and Γ_f^-.

Note that subscripts N and T identify the normal and tangential components of a vector quantity with respect to the discontinuity Γ_f. Since the static Coulomb law is adopted, the tangential velocity $\dot{\boldsymbol{g}}_T$ in (1h) can be replaced—at every timestep if an implicit time-marching scheme is used—with the tangential displacement increment in a discrete setting.

In our framework, the fracture is explicitly modeled according to a Discrete Fracture Model, with Γ_f describing the whole region where opening or contact may take place at any $t \in \mathbb{T}$ (Laursen, 2003). That is, we assume Γ_f is fixed and does not propagate. We need to solve for its (non-overlapping) partitioning into stick (Γ_f^{stick}), slip (Γ_f^{slip}) and open (Γ_f^{open}) patches at a given point in time. These three modes are associate with behavior regimes, namely:

- **Stick mode**: the discontinuity is fully closed and compressed with the Coulomb criterion satisfied The conductivity is constant and equal to $C_{f,0}$.
- **Slip mode**: the normal traction component t_N is unknown, i.e., there is continuity in the normal component, but a slip displacement $\boldsymbol{g}_T$ between Γ_f^+ and Γ_f^- is allowed for. The tangential component has magnitude $||\boldsymbol{t}_T^*||_2 = \tau_{\max}(t_N)$ and direction collinear with $\dot{\boldsymbol{g}}_T$. The conductivity behavior is the same as for the stick mode.
- **Open mode**: Γ_f^+ and Γ_f^- are not in contact and a free relative displacement $[\![\boldsymbol{u}]\!]$ is allowed for. In this case, the conductivity is related to the opening (see Eq. (2)).

Discrete formulation

We solve numerically the IBVP (1) using a mixed finite-element/finite-volume approach for the spatial discretization combined with a fully-implicit time-marching scheme. In particular, we address the contact mechanics problem using the saddle point formulation (Laursen, 2003; Wriggers, 2006) with the additional primary variable represented by the tractions acting on Γ_f. For the fluid flow simulation in the discontinuity, a finite volume method (Eymard et al., 2000) is adopted. Specifically, we use trilinear finite elements for the continuous displacement field, cell-centered piecewise-constant Lagrange multiplier and pressure fields, and the classical two-point flux approximation.

Solution strategy

The discrete form of the IBVP (1) consists of a nonlinear system of equations and inequalities in the unknowns $\mathbf{u}_n$ (nodal displacement), $\mathbf{t}_n$ (face tractions), and $\mathbf{p}_n$ (face pressure), where the subscript n denotes the discrete time level. However, introducing the active contact regions $\Gamma_{f,n}^{\text{stick}}$ and $\Gamma_{f,n}^{\text{slip}}$ at t_n, the inequalities (1d)-(1h) can be replaced with a variational equality. The discrete problem can be recast as a nonlinear system of equations that can be solved for the latest solution vectors $\mathbf{u}_n$, $\mathbf{t}_n$, and $\mathbf{p}_n$,

$$\begin{cases} \mathbf{r}_u(\mathbf{u}_n, \mathbf{t}_n, \mathbf{p}_n) = \mathbf{0}, \\ \mathbf{r}_t(\mathbf{u}_n, \mathbf{u}_{n-1}, \mathbf{t}_n) = \mathbf{0}, \\ \mathbf{r}_p(\mathbf{u}_n, \mathbf{u}_{n-1}, \mathbf{p}_n) = \mathbf{0}, \end{cases} \tag{3}$$

with $\mathbf{u}_{n-1}$ the known discrete displacement solution from the previous time step. The partition of $\Gamma_{f,n}$ into $\Gamma_{f,n}^{\text{stick}}$, $\Gamma_{f,n}^{\text{slip}}$ and $\Gamma_{f,n}^{\text{open}}$ at t_n is not known *a priori* and to advance one time step an iterative procedure that includes a Newton method-based solver applied to residual equations (3) is needed.

In this work, we solve the contact problem using an *active-set* strategy (Nocedal and Wright, 2006). In practice, first we assign an initial status to all the Lagrange multipliers and solve the discrete nonlinear problem (3). The initial state is the previous time step solution. Once the nonlinear problem is solved, the status of all Lagrange multipliers is checked and the subdivision into stick, slip, and open portions is accordingly updated. If at least one multiplier changes status, we solve a new nonlinear system and check the consistency of the outcome again. The procedure stops when the starting subdivision of Γ_f is consistent with the solution of the nonlinear problem.

Stabilization

The proposed stabilization procedures is first derived focusing on the stick-contact problem, in the absence of frictional slip or fluid flow. Later, the generalization to the complete set of cases/unknowns is discussed.

In pure stick conditions, i.e. $\Gamma_f = \Gamma_f^{\text{stick}}$, linearization of (3) yields the Jacobian system

$$\begin{bmatrix} K & C \\ C^T & 0 \end{bmatrix} \begin{bmatrix} \delta \mathbf{u} \\ \delta \mathbf{t}_S \end{bmatrix} = - \begin{bmatrix} \mathbf{r}_u \\ \mathbf{r}_S \end{bmatrix}, \tag{4}$$

with K the stiffness matrix associated to the bulk material and C the coupling term between displacement and traction fields. For this saddle point system, stability requires the displacement and traction spaces satisfy the discrete inf-sup condition (Brezzi and Bathe, 1990). Unfortunately, a trilinear interpolation for the displacement combined with a face-centered piecewise constant Lagrange multiplier interpolation does not uniformly satisfy the inf-sup condition, leading to unstable approximations (Wohlmuth, 2011, Section 3.1).

The proposed stabilization technique follows the macroelement approach, as described in Elman et al. (2014). In our case, the macroelement is formed by two interface elements ($\varphi_i, i = \{1,2\}$) and four quadrilaterals ($\tau_k, k = \{1,\dots,4\}$), two for each side of the fracture (see Fig. 2a). Note that the displacement is fixed for the ten nodes on the macroelement boundary. The objective is to derive a stabilization that produces a well-posed problem by investigating the kernel modes of the Schur complement for the Lagrange multipliers. Performing an eigen-decomposition of the Schur complement of the matrix in Eq. (4), a basis for the null space is identified as:

$$\mathbf{v}_1 = \begin{bmatrix} 1 & 0 & -1 & 0 \end{bmatrix}^T, \qquad \mathbf{v}_2 = \begin{bmatrix} 0 & 1 & 0 & -1 \end{bmatrix}^T. \tag{5}$$

We observe that the kernel of S represents the *checkerboard* mode for the traction normal- and tangential-component, respectively. To remove the source of the macroelement instability, we could introduce a symmetric and positive semi-definite matrix $H^* = VV^T$, with V the matrix having columns $\mathbf{v}_1$ and $\mathbf{v}_2$. On the downside, a proper scaling to match the eigenspectrum of the physical Schur complement is needed (Elman et al., 2014). This scaling must incorporate both mechanical and geometric information. Its definition may become quite cumbersome in the presence of distorted grids and material heterogeneity. Instead, we pursue an algebraic approach that overcomes the need for a scaling factor. We rely on matrices K and C in (4), which already contain the necessary geometric and material property information.

In the classic macroelement approach, both mechanical and geometric information are summarized by the scaling factor α that, for distorted grids and material heterogeneity, can be difficult to define. To overcome this scaling factor, the authors in Franceschini et al. (2020) proposed an algebraic alternative for computing the stabilization matrix at the macroelement level. Here, we recall just the basic characteristics of the method, useful to define our new approach. For any details, we refer the reader to Franceschini et al. (2020).

For the two dimensional patch of interface elements of Fig. 2b, the coupling matrix C given in Eq. (4) reads

$$C = \begin{bmatrix} \tilde{\ell}_1 R_2 & \tilde{\ell}_2 R_2 \\ -\tilde{\ell}_1 R_2 & -\tilde{\ell}_2 R_2 \end{bmatrix}, \tag{6}$$

where $\tilde{\ell}_1$ and $\tilde{\ell}_2$ are the interface element lengths associated to the vertex in common between elements φ_1 and φ_2, i.e. the integral of the standard basis function associated to that vertex over φ_1 and φ_2, respectively. The *building block* for the algebraic stabilization is the following $\widetilde{C}$ matrix, which rows are formed from C, swapping block columns and changing sign to the first block column,

$$\widetilde{C} = \begin{bmatrix} -\tilde{\ell}_2 R_2 & \tilde{\ell}_1 R_2 \\ \tilde{\ell}_2 R_2 & -\tilde{\ell}_1 R_2 \end{bmatrix}. \tag{7}$$

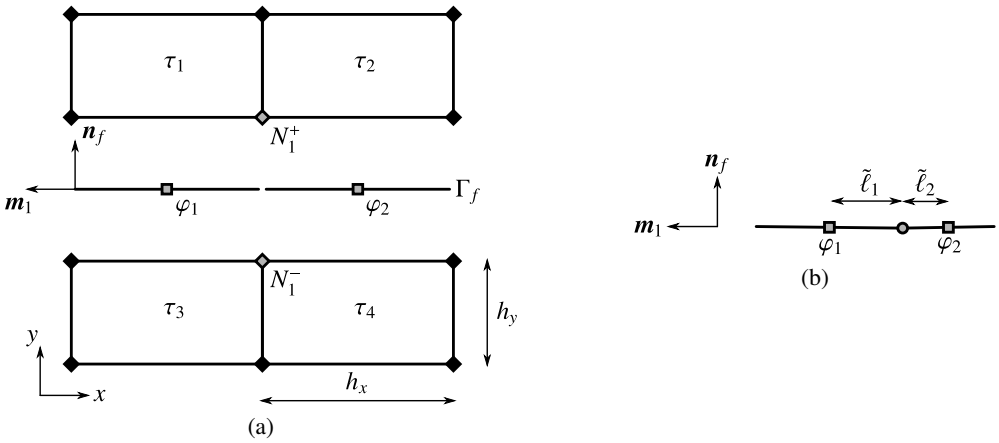

Figure 2: Location of displacement (◆) and traction (■) degrees of freedom (DOFs) for a 2D macroelement. Black and gray identify fixed and active DOFs, respectively (a); general interface element patches for a 2D macroelement. Squares (■) indicate the barycenter of the interface elements. Quantities $\tilde{\ell}_i$, $i \in \{1,2\}$ denote the length associated to the common vertex (●) (b).

The natural choice for the scaling is the inverse of the stiffness matrix in Eq. (4), i.e. K^{-1}, being that $\widetilde{C}$ has the same entries of C, except for the order (they are swapped on a Lagrange multiplier base) and the sign. Therefore, a macroelement stabilization matrix can be define as $H = \widetilde{C}^T D_{\widetilde{K}}^{-1} \widetilde{C}$.

A quite natural way to overcome the inherent limitations of a macroelement-based scheme, i.e., the need for a certain mesh topology, is to simply apply the algebraic stabilization to all pairs of interface elements, as opposed to macroelement-internal edges only. Again, this approach is widely described in (Franceschini et al., 2020). The new strategy exploits the fact that the global stabilization is quite similar to a finite volume scheme in the sense that the Lagrange multiplier is a cell-centered field and we need to stabilize the displacement jump across interfaces between cells. In the classical two-point flux approximation (TPFA) approach, fluxes between cells are computed across interfaces (points in 2D, edges in 3D). Thus, the main idea is to find a parallelism with the transmissibility, i.e., a compliance function of geometric and physical quantities. The reason to look for a compliance instead of a stiffness is because the stabilization matrix is a contribution to the Schur complement, that contains the inverse of the stiffness matrix.

Referring to Fig. 2, the coupling matrix C is given in Eq. (6) and following what proposed in the local algebraic approach, the null kernel to be stabilized is shown in Eq. (7). The *lumped* stiffness matrix, i.e., the result of the local gathering, is:

$$K_D = \operatorname{diag}\left(\begin{bmatrix} K_t & K_b \end{bmatrix}\right), \tag{8}$$

where K_t is the diagonal local stiffness matrix for the common node on the *top* side of the fracture (opposite to the *bottom* one). The stabilization contribution for this couple is $H = \widetilde{C}^T K_D^{-1} \widetilde{C}$ and reads

$$\begin{bmatrix} \ell_2^2 \left(R_2^T \left(K_t^{-1} + K_b^{-1}\right) R_2\right) & -\ell_1 \ell_2 \left(R_2^T \left(K_t^{-1} + K_b^{-1}\right) R_2\right) \\ -\ell_1 \ell_2 \left(R_2^T \left(K_t^{-1} + K_b^{-1}\right) R_2\right) & \ell_1^2 \left(R_2^T \left(K_t^{-1} + K_b^{-1}\right) R_2\right) \end{bmatrix}. \tag{9}$$

From the definition of extradiagonal terms $H_{12} = H_{21}^T$ we can recognize a sort of transmissibility, i.e., a function of geometry and physical parameter averaged on the two elements. It is enough now to approximate the local gathering from the stiffness matrix with a direct relation based on elastic parameters. From the macroelement analysis, we know the relation between (E, ν) and the non trivial eigenvalues. Simplifying it, we can write:

$$K_t = \frac{1}{2}\left(\frac{E}{(1+\nu)(1-2\nu)} \frac{1}{3}(3-4\nu)\Big|_{1,t} A_{1,t} l_{1,t}^{-2} + \frac{E}{(1+\nu)(1-2\nu)} \frac{1}{3}(3-4\nu)\Big|_{2,t} A_{2,t} l_{2,t}^{-2} \right), \tag{10}$$

where $A_{1,t}$ is the element area and $l_{1,t}$ is a 2×2 diagonal matrix containing the dimension of the box inscribing the finite element on the top side of interface element number 1, i.e.:

$$l_t = \text{diag}\left(\left[\max(x) - \min(x) \quad \max(y) - \min(y)\right]\right), \tag{11}$$

where x and y are nodal coordinates for the given element. The definition of Eq. (10) is extended to the other element, approximating the remaining lumped stiffness matrices, i.e., K_b. Thus, for the node shared by two elements it is enough to compute the following quantity, function of geometric quantities and elastic parameters:

$$\Upsilon = \ell_1 \ell_2 \left(R_2^T \left(K_t^{-1} + K_b^{-1}\right) R_2\right), \tag{12}$$

then, for the couple of elements of Fig. 2, we have that the local matrix to assemble is:

$$H_{\text{loc}} = \begin{bmatrix} \Upsilon & -\Upsilon \\ -\Upsilon & \Upsilon \end{bmatrix}. \tag{13}$$

The same procedure has to be repeated for all the interfaces (points in 2D, edges in 3D) shared by two elements. The extension to the 3D case is straightforward. Comparing this approach with the global stabilization, no sensible differences are registered.

Given the easier implementation in a highly parallel MPI-based simulator and the almost identical result with the algebraic global stabilization, the latter approach is adopted as default choice in this work. The main limitation of the algebraic global method in a distributed-memory simulator regards its need of access rows and columns of assembled matrices and the fact that these can be spread over different processes. Instead, using the new approach, computations can be done at a local level, without employing any additional communication.

Dealing with friction and fluid flow

The methods described for the stick problem form the building blocks for stabilizing the full physical model, allowing for frictional sliding and fluid flow. It is enough to remember that only the three traction components for the stick elements and the normal component for the sliding elements are primary unknown and require the stabilization. The tangential components in case of sliding as well the traction itself in case of opening elements are known. The pressure acts as the normal component of the traction, thus the gathering of the stabilization matrix components associated to normal degrees-of-freedom is enough to stabilize the pressure field.

Results

We demonstrate the performances of the presented modeling approach for the new stabilization scheme. A vertical fracture, tilted by 20° in the horizontal plane, is embedded in a 3D body (see Fig. 3a), passing it from top to bottom. A linearly increasing in time flow rate (Q) is injected in the middle of the fracture (see Fig. 3b), while the fracture sides are kept to constant pressure ($p_0 = 0$). The top and bottom surfaces of the 3D body are constrained in the z-direction, while only one column of nodes on each side is constrained in x- and y-direction, according to the side, to be consistent with the symmetry condition (excluding the fracture). An external constant load $\sigma_0 = 100$ Mpa is applied as shown in Fig. 3a. This is not enough to trigger fracture sliding. The simulation consists of 20 time steps of 1 s, with a total flow rate increasing from 0 up to $Q = 2 \cdot 10^{-4}$ m^3/s after 10 s and then decreasing down to 0 again. The rock material is characterized by a linear elastic behaviour, with Young's modulus $E = 3 \cdot 10^4$ MPa and Poisson's ratio $\nu = 0.25$. The fracture has a constant friction angle of 30°. Neither cohesion nor initial stress are present. Following Kamenov et al. (2013), the initial conductivity value (see Eq. (2)) is $C_{f,0} = 10$ mD $\cdot$ m $= 9.87 \cdot 10^{-15}$ m$^2 \cdot$ m. The domain size is $10 \times 10 \times 0.5$ m and the fracture length is 2 m. The computational domain consists of 8096 nodes, 6820 elements and 400 interface elements.

Fig. 4 shows the behavior of the fracture during the entire simulation, in terms of number of elements in stick, slip and open state. As one can expect, the number of open elements reflect the external source term time-dependency, with a peak of 320 elements attained when the flow rate reaches its maximum.

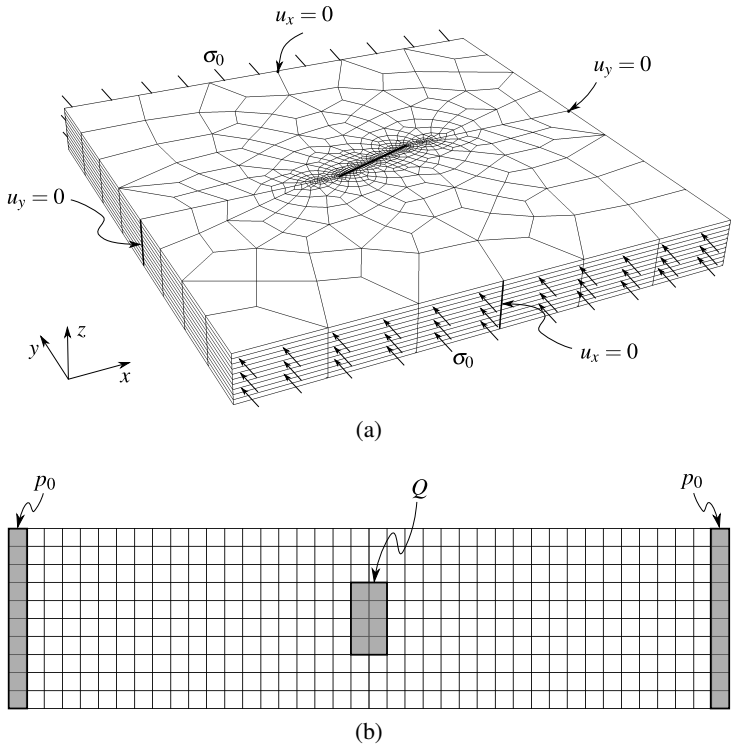

Figure 3: View of the 3D domain, with the fracture trace highlighted (a). Front view of the fracture plane only, with injection location and fixed boundary conditions for pressure (b).

During the first half of the simulation, the pressure always increases, reducing the normal component of the traction (being the external load constant) and thus more and more elements start sliding. After 10 s, pressure drops, the normal strength increases and all the sliding elements are glued together, recovering a stick condition. In Fig. 4 there are also the trend over time of both opening and sliding for a location in the center of the fracture. Sliding increases up to the maximum value corresponding to the maximum injection rate, which is not recovered as the overpressure dissipates because of the increased normal strength. Fig. 5 shows the average values for the fluid pressure and the normal component of the traction on the entire fracture for all the time steps. As already observed, the behavior follows the symmetric external flow forcing term and the two quantities are complementary to each other.Finally, in Fig. 5 the pressure profiles on the middle section of the fracture (contained in the x-y plane) for different time steps are shown. At the beginning, the profile is almost linear, as the conductivity is constant and equal to $C_{f,0}$. As the simulation proceeds, the profile flattens, with an almost constant value in the center part, where the conductivity is higher because of the opening contribution.

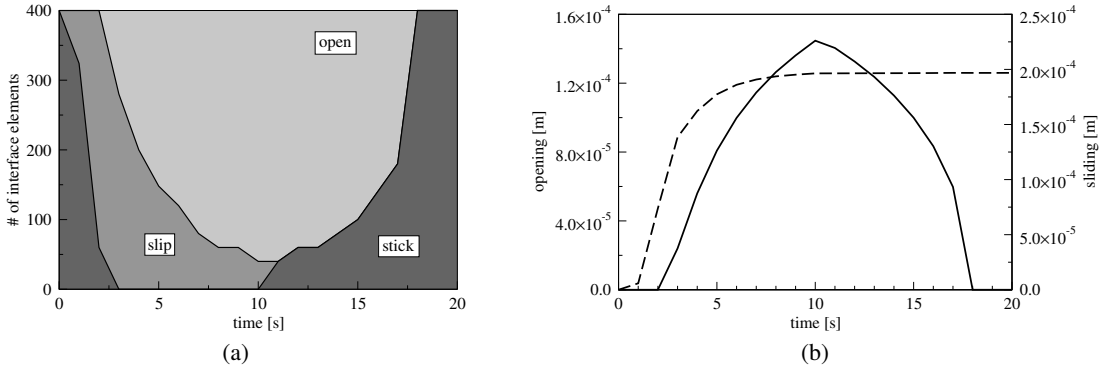

Figure 4: Number of interface elements for each fracture state during the entire simulation (a); opening (continuous line) and sliding (dashed line) in the center of the fracture for all time steps (b).

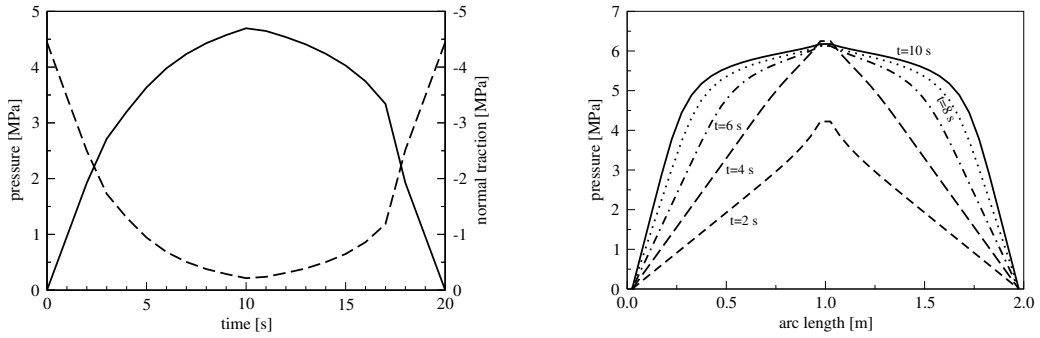

Figure 5: Average pressure (continuous line) and normal component of traction (dashed line) on the entire fracture for all times (a); pressure profiles on the middle section of the fracture (orthogonal to z-axis) for different time steps (b).

From the algebraic standpoint, we can compare the eigenspectrum of the original Schur complement for the traction variables, i.e., $S = -C^T K^{-1} C$, with reference to Eq. (4), and the one relative to the stabilized Schur complement, i.e., $S = H_S - C^T K^{-1} C$, when all the elements are in the stick condition. Fig. 6 shows the two eigenspectra (in the plot we actually report -λ, with λ a generic eigenvalue, as both matrices are symmetric negative definite). We notice that the original Schur complement is singular, with an effective conditioning of $\lambda_{\max}/\lambda_{\min>0} = 6.83 \cdot 10^5$, while the stabilized one is a regular matrix, with a conditioning of $\lambda_{\max}/\lambda_{\min} = 67.33$. The two profiles coincide for the largest eigenvalues, but diverge substantially when moving towards the minimal eigenvalues. Finally, in Fig. 6 we report the convergence profile for the sixth time step of the adaptive nonlinear algorithm, that is a combination of an outer active set loop and an inner Newton loop. Once a Newton loop ends, the solution is used to update the fracture partitioning into stick, slip and open elements and, with this new subdivision, the next Newton loop is started. The procedure continues up to when no elements change status.

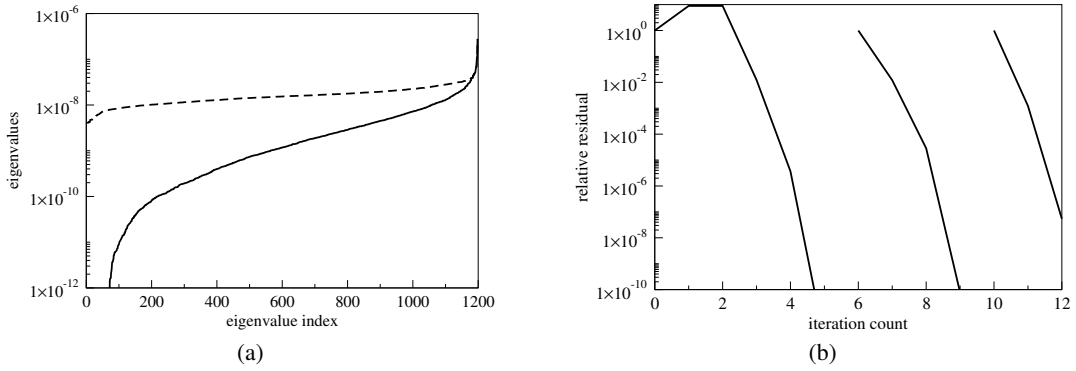

Figure 6: Eigenspectra for both the unstabilized Schur complement (which is singular) and the stabilized Schur complement (a); convergence profile for the nonlinear strategy used in this work for the sixth step (b).

Conclusions

In this work, we have considered the problem of quasi-static contact mechanics coupled with fracture fluid flow, using a mixed lowest order finite-element/finite-volume representation. This choice has the advantage that a single computational grid is employed and any interpolation between fields can be avoided. Nevertheless, this approach does not automatically satisfy the discrete inf-sup stability condition and requires a stabilization contribution. Starting from a macroelement approach, we developed a new strategy that overcome some limitations of classic macroelement schemes. A synthetic example is presented to illustrate the merits of the proposed stabilization strategies. The global nonlinear problem is

solved using an outer active set strategy combined with an inner Newton's method. Future developments of this work will include extension to fluid flow in the matrix, more complex fracture networks, and the development of efficient solvers for the resulting linear systems.

Acknowledgements

Funding was provided by TOTAL S.A. through the FC-MAELSTROM project. Portions of this work were performed under the auspices of the U.S. Department of Energy by Lawrence Livermore National Laboratory under Contract DE-AC52-07-NA27344.

References

Brezzi, F. and Bathe, K.J. [1990] A discourse on the stability conditions for mixed finite element formulations. *Comput. Meth. Appl. Mech. Eng.*, **82**(1-3), 27–57.

Deb, D. and Das, K.C. [2010] Extended finite element method (XFEM) for analysis of cohesive rock joint. *Geotech. Geol. Eng.*, **28**(5), 643–659.

Deb, R. and Jenny, P. [2017] Modeling of shear failure in fractured reservoirs with a porous matrix. *Comput. Geosci.*, **21**(5), 1119–1134.

Elman, H.C., Silvester, D.J. and Wathen, A.J. [2014] *Finite elements and fast iterative solvers: with applications in incompressible fluid dynamics*. Oxford University Press, USA.

Eymard, R., Gallouët, T. and Herbin, R. [2000] Finite Volume Methods. In: Ciarlet, P.G. and Lions, J.L. (Eds.) *Handbook of Numerical Analysis*, 7, Elsevier, 713–1018.

Franceschini, A., Castelletto, N., White, J.A. and Tchelepi, H.A. [2020] Algebraically stabilized Lagrange multiplier method for frictional contact mechanics with hydraulically active fractures. *Comput. Methods Appl. Mech. Eng.*, **368**.

Garipov, T.A., Karimi-Fard, M. and Tchelepi, H.A. [2016] Discrete fracture model for coupled flow and geomechanics. *Comput. Geosci.*, **20**(1), 149–160.

Goodman, R.E., Taylor, R.L. and Brekke, T.L. [1968] A model for the mechanics of jointed rock. *Journal of Soil Mechanics & Foundations Div.*, **94**, 637–659.

Kamenov, A., Zhu, D., Hill, A.D. and Zhang, J. [2013] Laboratory measurement of hydraulic fracture conductivities in the Barnett shale. In: *SPE Hydraulic Fracturing Technology Conference*. Society of Petroleum Engineers, 216–227.

Kikuchi, N. and Oden, J.T. [1988] *Contact Problems in Elasticity: A Study of Variational Inequalities and Finite Element Methods*. Society for Industrial and Applied Mathematics, Philadelphia, PA, USA.

Laursen, T.A. [2003] *Computational Contact and Impact Mechanics: Fundamentals of Modeling Interfacial Phenomena in Nonlinear Finite Element Analysis*. Springer-Verlag Berlin Heidelberg.

Nocedal, J. and Wright, S. [2006] *Numerical optimization*. Springer Science & Business Media.

Rutqvist, J., Wu, Y.S., Tsang, C.F. and Bodvarsson, G. [2002] A modeling approach for analysis of coupled multiphase fluid flow, heat transfer, and deformation in fractured porous rock. *Int. J. Rock Mech. Min. Sci.*, **39**(4), 429–442.

Shakiba, M. and Sepehrnoori, K. [2015] Using embedded discrete fracture model (EDFM) and microseismic monitoring data to characterize the complex hydraulic fracture networks. In: *SPE annual technical conference and exhibition*. Society of Petroleum Engineers, 1–23.

Silvester, D.J. and Kechkar, N. [1990] Stabilised bilinear-constant velocity-pressure finite elements for the conjugate gradient solution of the Stokes problem. *Comput. Meth. Appl. Mech. Eng.*, **79**(1), 71–86.

Verhoosel, C.V. and de Borst, R. [2013] A phase-field model for cohesive fracture. *Int. J. Numer. Methods Eng.*, **96**(1), 43–62.

Wheeler, M.F., Wick, T. and Wollner, W. [2014] An augmented-Lagrangian method for the phase-field approach for pressurized fractures. *Comput. Methods Appl. Mech. Eng.*, **271**, 69–85.

Wohlmuth, B. [2011] Variationally consistent discretization schemes and numerical algorithms for contact problems. *Acta Numerica*, **20**, 569–734.

Wriggers, P. [2006] *Computational Contact Mechanics*. Springer-Verlag Berlin Heidelberg, 2nd edn.